

Deterministic and stochastic models of dislocation patterning

Ronghai Wu,¹ Daniel Tüzes,² Péter Dusán Ispánovity,² István Groma,² and Michael Zaiser^{1,3,*}

¹*Institute for Materials Simulation, Department of Materials Science,*

Friedrich-Alexander University Erlangen-Nürnberg (FAU), Dr.-Mack-Str. 77, 90762 Fürth, Germany

²*Department of Materials Physics, ELTE, Eötvös Loránd University, H-1517 Budapest POB 32, Hungary*

³*Department of Mechanics and Engineering, Southwest Jiaotong University, Chengdu, P.R. China*

We study a continuum model of dislocation transport in order to investigate the formation of heterogeneous dislocation patterns. We propose a physical mechanism which relates the formation of heterogeneous patterns to the dynamics of a driven system which tries to minimize an internal energy functional while subject to dynamic constraints and state dependent friction. This leads us to a novel interpretation which resolves the old 'energetic vs. dynamic' controversy regarding the physical origin of dislocation patterns. We demonstrate the robustness of the developed patterning scenario by considering the simplest possible case (plane strain, single slip) yet implementing the dynamics of the dislocation density evolution in two very different manners, namely (i) a hydrodynamic formulation which considers transport equations that are continuous in space and time while assuming a linear stress dependency of dislocation motion, and (ii) a stochastic cellular automaton implementation which assumes spatially and temporally discrete transport of discrete 'packets' of dislocation density which move according to an extremal dynamics. Despite the huge differences between both kinds of models, we find that the emergent patterns are mutually consistent and in agreement with the prediction of a linear stability analysis of the continuum model. We also show how different types of initial conditions lead to different intermediate evolution scenarios which, however, do not affect the properties of the fully developed patterns.

PACS numbers: 64.70.Pf, 61.20.Lc, 81.05.Kf, 61.72.Bb

I. INTRODUCTION

Ever since the first TEM observations of dislocations it is known that the arrangement of dislocations in deformed crystals is practically never homogeneous: dislocations show an intrinsic propensity to forming heterogeneous patterns. There is an equally long standing discussion regarding the physical nature of these patterns which is matched by an amazing variety of approaches to their modeling, many of which are based upon analogies with pattern formation in other physical systems. Thus, it has been argued that dislocation patterns can be understood as minimizers of some kind of (elastic) energy functional (see e.g. Hansen and Kuhlmann-Wilsdorf [1]). Unfortunately this 'energetic' approach to dislocation patterning has hardly ever been cast into a tangible mathematical framework by actually formulating and minimizing the energy functional in question, one notable exception being the work of Holt [2] which is clearly crafted in analogy with contemporary models of spinodal decomposition patterns and relates the patterning of dislocation densities to the minimization of an associated internal energy functional – a process which in stark contrast with experiment is predicted to occur even in the absence of external stress. The 'energetic' approach may be contrasted with the idea that dislocations in a deforming crystal constitute a driven system far from equilibrium where patterns may form as dissipative structures. This has led to the formulation of nonlinear sets of partial dif-

ferential equations for dislocation densities Walgraef and Aifantis [3], Pontes *et al.* [4] which give rise to a variety of interesting patterns. Some of these resemble dislocation patterns observed by TEM, while other types of patterns predicted by the same equations, such as spiral waves, have never been observed [5]. In our opinion most of these models suffer from an overly phenomenological approach to modelling: They aim at reproducing patterns (actually, pictures of patterns) rather than deriving them from the known elastic and kinematic properties of dislocation systems. As a consequence, the fundamental controversy whether dislocation patterning is in essence an energetic or a dynamic phenomenon, which has been neatly summarized by Nabarro [6], remains unresolved.

Only in recent years, attempts have been made to formulate dislocation density based models based upon averaging procedures which lead from the dynamics of discrete dislocations to the evolution of dislocation densities in a systematic manner. These methods have been used to formulate the kinematics of dislocations in 2D and lately in 3D [7–9] and also to systematically derive driving forces for the dynamics. To the latter end, two alternative approaches have been pursued: Driving forces for dislocation density evolution may be obtained by directly averaging the interaction forces of discrete dislocations [10–12]. Alternatively, one may formulate an energy functional governing the dynamics based upon phenomenological considerations [13, 14] or from direct averaging of the elastic energy of the discrete dislocation system [15], and then obtain driving forces from variation of the energy functional in conjunction with thermodynamic consistency requirements [16]. Both approaches

* michael.zaiser@fau.de

have been shown to yield mutually consistent results provided that, in the variational approach, a nontrivial mobility function is assumed which implements a friction stress [12].

Importantly, these statistical averaging approaches do not pursue the primary aim of 'modelling patterning', i.e., of reproducing experimental images in a more or less faithful manner. Rather, such models aim at 'modelling dislocations': their primary thrust is to provide an adequate representation of the motion and interactions of dislocations in a continuum framework ('continuum dislocation dynamics', CDD). However, it has soon become clear that in CDD models the emergence of heterogeneous dislocation patterns turns out to be an almost inevitable feature of the collective dynamics. Simulations of CDD models in 3D demonstrate an intrinsic tendency towards dislocation patterning [17, 18] as they relate the emergence of patterning to the same dislocation interactions that govern strain hardening, in line with the 'principle of similitude' [19]. This principle has been related to fundamental invariance properties of the equations that govern the properties of discrete dislocation systems, and indeed all physically based models of dislocation patterning published in recent years are consistent with these invariance properties [20].

While most recent models exploit advances in computational power [18] or in kinematic averaging methods [17] in order to address the important problem of dislocation patterning in 3D and under conditions of multiple slip, the present authors have pursued a more simplistic yet more fundamental goal, namely to elucidate the respective influences of dynamic and energetic mechanisms on the patterning process. To this end we focus on a minimal system (2D, single slip) where an exact representation of the kinematics is possible and well-defined forms have been established both for the energy functional [13, 15] and also for the effective mobility law [12]. As a consequence, we can dispense to a large extent of phenomenological assumptions and obtain a complete understanding of the interplay of energy minimization, external driving, and friction in driving the emergence of dislocation patterns. In a previous work [12] we had analyzed the linear stability of the ensuing equations. While this allowed to reach important conclusions regarding the patterning mechanism, a linear stability analysis is of necessity insufficient to decide upon the stability of the emergent patterns and the robustness of the patterning scenario. We therefore, in the present paper, complete this with a comprehensive study of nonlinear aspects of patterning including the influence of initial condition, pattern growth mode, and investigation of pattern stability as well as an investigation of the influences of model implementation (continuous vs. discrete, deterministic vs. stochastic). The paper is organized as follows: In Section 2, we briefly present the continuum model formulated by Groma *et al.* [12] and its implementation in a spatially and temporally continuous setting. Section 3 presents a spatially and temporally discrete,

stochastic model which considers the same spatial couplings and friction rules, but implements a completely different dynamics. Results from both models are presented in Section 4 and compared to results from linear stability analysis. A discussion concerning the nature and robustness of dislocation patterning is presented in the Conclusions.

II. DETERMINISTIC CONTINUUM MODEL

In the following we give a brief summary of the continuum model of dislocation transport developed in Groma *et al.* [12], see also Valdenaire *et al.* [11]. For a detailed discussion of the derivation and statistical averaging methodology the reader is referred to the original works of Groma *et al.* [10], Valdenaire *et al.* [11], Groma *et al.* [12]. We consider a 2D system of straight parallel edge dislocations of both signs which can be envisaged as charged point particles moving in a perpendicularly intersecting plane (taken to be the xy plane). Dislocations of Burgers vector modulus b are assumed to move on a single slip system which constrains their motion to the slip direction which we identify with the x direction.

A. Transport equations

The model equations have the structure of continuity equations. The stress-driven motion of a dislocation depends on its sign; we use the sign convention that, under a positive resolved shear stress, positive dislocations of density ρ^+ move with velocity v^+ in the $+x$ and negative dislocations of density ρ^- move with velocity $-v^-$ in the $-x$ direction. These motions produce a shear strain γ at rate

$$\partial_t \gamma = b (\rho^+ v^+ + \rho^- v^-) \quad (1)$$

Neglecting dislocation generation or annihilation, the transport equations have the simple structure

$$\begin{aligned} \partial_t \rho^+(\mathbf{r}, t) &= -\partial_x (\rho^+ v^+) \\ \partial_t \rho^-(\mathbf{r}, t) &= \partial_x (\rho^- v^-) \end{aligned} \quad (2)$$

where

$$\begin{aligned} v^+(\mathbf{r}, t) &= M_0 b \mathcal{T}^+(\mathbf{r}, t) \\ v^-(\mathbf{r}, t) &= M_0 b \mathcal{T}^-(\mathbf{r}, t). \end{aligned} \quad (3)$$

In these equations, the \mathcal{T}^\pm are effective shear stresses driving the motion of positive and negative dislocations and M_0 is a dislocation mobility coefficient (inverse drag coefficient). Hence, we assume the dislocation velocities to be proportional to the effective driving forces $\mathcal{T}^\pm b$ (i.e., the effective glide components of the Peach-Koehler forces).

B. Evaluation of the effective driving stresses

The effective driving stresses $\mathcal{T}(\tau_d^\pm, \tau_f^\pm)$ result from the combination of sign-dependent local driving stresses τ_d^\pm and friction stresses τ_f^\pm as

$$\mathcal{T}(\tau_d, \tau_f) = \text{sign}(\tau_d) (|\tau_d| - \tau_f) \quad (4)$$

The driving stresses are given by combinations of a spatially homogeneous shear stress τ_{ext} arising from remotely applied boundary tractions which provides the external driving force for dislocation motion and plastic flow, and a set of stress contributions describing dislocation interactions,

$$\tau_d^\pm = \tau_{\text{ext}} + \tau_{\text{int}} + \tau_{\text{back}} \pm \tau_{\text{diff}}. \quad (5)$$

We discuss the interaction stress contributions τ_{int} , τ_b , and τ_d in turn:

1. The 'internal' shear stress τ_{int} arises from heterogeneity of the plastic eigenstrain $\epsilon_{\text{pl}} = \gamma(\mathbf{e}_x \otimes \mathbf{e}_y + \mathbf{e}_y \otimes \mathbf{e}_x)/2$. This stress can be calculated in various manners, e.g. by direct convolution of the dislocation shear stress field with the excess dislocation density $\kappa = \rho^+ - \rho^- = -\partial_x \gamma/b$ as done by Groma *et al.* [10], by using an Airy stress function formalism [13], or numerically by solving the eigenstrain problem using finite elements. In the following we adopt a fourth method where we calculate the internal stress directly from the plastic strain γ using a Green's function formalism as adopted in Zaiser and Moretti [21],

$$\tau_{\text{int}}(\mathbf{r}) = \int \gamma(\mathbf{r}') \mu(\mathbf{r} - \mathbf{r}') d^2 r' \quad (6)$$

where μ is an interaction kernel function with the Fourier transform

$$\mathcal{G}(\mathbf{k}) = \frac{\mu}{\pi(1-\nu)} \frac{k_x^2 k_y^2}{k^4} = \mu T(\mathbf{k}), \quad (7)$$

where μ is the shear modulus of the material, ν is Poisson's ratio, and k_x and k_y are components of the Fourier wavevector with modulus k .

2. The 'back stress' τ_{back} counter-acts accumulation of dislocations of the same sign. It is given by

$$\tau_b(\mathbf{r}) = -\mu b \frac{D}{\rho} \partial_x \kappa(\mathbf{r}) = \mu \frac{D}{\rho} \partial_{xx} \gamma(\mathbf{r}), \quad (8)$$

where D is a nondimensional factor of the order of unity and $\rho = \rho^+ + \rho^-$ is the total dislocation density. We see that the back stress is proportional to the second gradient of the shear strain.

3. Finally, the 'diffusion stress' τ_{diff} is given by

$$\tau_{\text{diff}}(\mathbf{r}) = -\mu b \frac{A}{\rho} \partial_x \rho(\mathbf{r}), \quad (9)$$

where A is another nondimensional factor of the order of unity. The terminology 'diffusion stress' is used because this stress, if inserted via Eqs (5), (4), (3) into the transport equations Eq. (2), gives rise to a diffusion-like contribution to the evolution of the total dislocation density ρ .

Groma *et al.* [12] observed that the stress contributions τ_{int} , τ_{back} and τ_{diff} represent kinematic hardening contributions. Indeed all these stress contributions can, via variational calculus, be derived from an energy functional of the dislocation system given by

$$\begin{aligned} E &= E_{\text{el}} + E_{\text{dis}}, \\ E_{\text{el}} &= \int \int \gamma(\mathbf{r}) \mathcal{G}(\mathbf{r} - \mathbf{r}') \gamma(\mathbf{r}') d^2 r d^2 r', \\ E_{\text{dis}} &= \int \mu b^2 \left(A \rho \ln(\rho) + \frac{D}{2} \frac{\kappa^2}{\rho} \right) d^2 r. \end{aligned} \quad (10)$$

The first contribution to this functional represents the elastic energy associated with the average plastic eigenstrain γ , whereas the second term represents a correction which captures elastic energy contributions due to stress and strain heterogeneities on the scale of single dislocations, which cannot be represented in terms of the coarse grained strain variable γ . For a formal derivation of these terms by averaging the elastic energy of the underlying discrete dislocation system, see Zaiser [15].

The 'friction stresses' τ_f^\pm in the effective stress expressions (4) are given by

$$\tau_f^\pm = \alpha \mu b \sqrt{\rho} \left(1 \mp \frac{\kappa}{\rho} \right). \quad (11)$$

These stresses are of a different nature from the driving stresses: they represent friction-like, isotropic hardening contributions. While these stresses arise naturally from direct averaging of the dislocation interactions, they cannot be derived from an energy functional but need to be added 'by hand' to an energy-based formalism where they enter in terms of a non-trivial, nonlinear mobility function with a mobility threshold [12]. The functional form of these stresses is that of Taylor stresses; in physical terms, they represent the mutual trapping of positive and negative dislocations into dipolar or multipolar configurations. Their dependency on κ reflects the fact that the presence of an excess of dislocations of one sign implies reduced pinning of the majority and enhanced pinning of the minority population. In particular, for $\kappa = \rho$ or $\kappa = -\rho$ (only positive or only negative dislocations) the pinning stress is zero.

C. Initial conditions, boundary conditions, loading protocol

We implement periodic boundary conditions in x and y for the stresses, and in x for the dislocation fluxes. For the stresses this means that the convolution integral

in Eq. (6) is evaluated using the L -periodically continued Fourier transform of the kernel. As initial conditions we use $\rho^\pm(\mathbf{r}, t) = \rho_0/2 + \epsilon\delta\rho^\pm(\mathbf{r}, t)$ where $\epsilon \ll 1$ and we consider two types of perturbation $\delta\rho^\pm$: (1) a Gaussian white noise of unit amplitude and (2) a localized Gaussian 'blob' of width $l = \rho_0^{-1/2}$ located at the center of the simulation cell. The loading protocol is simple: We impose a constant external stress and keep it fixed throughout the simulation, thus implementing creep-like testing conditions.

III. DISCRETE STOCHASTIC MODEL

Our second model considers dislocation motion to be driven by the same stress contributions as introduced in Section 2B. However, the implementation of the dynamics differs radically.

We now consider a spatially and temporally discrete model where space is discretized onto a $L \times L$ lattice consisting of $N \times N$ square unit cells of size $d \times d$ with $d = L/N$. The simulation lattice is aligned with the x and y axes of a Cartesian coordinate system where, $(x, y) \rightarrow (i = x/d, j = y/d)$. The discrete coordinate i marks the slip direction and j the direction of the slip plane normal. Periodic boundary conditions are assumed. Again we consider densities ρ^\pm of positive and negative dislocations, however, dislocation densities are now assumed to be constant over each lattice cell and to be 'quantized' in units ρ_d^\pm which are integer fractions $\rho_d^\pm = \rho_0/(2M)$ of the overall dislocation density ρ_0 . A discrete density quantum ρ_d of sign $s \in \{1, -1\}$ is henceforth denoted as a positive or negative 'dislocatom'. The dislocation state of lattice site (i, j) is then characterized by the densities $\rho_{ij}^+ = n_{ij}^+\rho_d$ and $\rho_{ij}^- = n_{ij}^-\rho_d$ or equivalently by the respective dislocatom numbers. Again, we consider the overall densities of positive and negative dislocations and hence the total dislocatom numbers to be conserved.

We evolve the quantized dislocation densities on the lattice in discrete steps. Since all dependent and independent variables of the problem can be expressed in terms of integer numbers, we are dealing with a cellular automaton (CA) dynamics for which we now specify the evolution rules.

A. Cellular automaton dynamics

The motion of dislocations is described as discrete shuffling of dislocatoms between sites that are adjacent in i direction. Motion of positive and negative dislocatoms is controlled by driving forces which are proportional to the same effective stresses \mathcal{T}^\pm that govern dislocation transport in the continuum model, with the only difference that these stresses (and also the plastic strains) are now defined on the boundaries between cells (i, j) and $(i+1, j)$ that are adjacent in the slip direction. This implies that

the lattice used for stress evaluation is shifted with respect to the lattice used for dislocation density evolution by $d/2$ along the direction of slip. Without loss of generality, we denote as boundary (i, j) the boundary between cells (i, j) and $(i+1, j)$.

Dislocatoms move across boundaries subject to the following rules:

- Dislocatoms do not move across boundaries experiencing zero effective stress.
- Among all boundaries experiencing non-zero effective stress we determine, in each given time step, a critical boundary and dislocatom sign defined as the boundary and sign for which the effective stress has the largest absolute value:

$$(i_m, j_m, s_m) : |\mathcal{T}_{i_m j_m}^{s_m}| := \max_{i,j,s} |\mathcal{T}_{ij}^s|. \quad (12)$$

Across this critical boundary, we move one dislocatom of sign s_m in direction $s_m \text{sign}(\mathcal{T}_{i_m j_m}^{s_m})$. In other words, positive dislocatoms move to the right from site $(i \rightarrow i+1)$ under a positive stress and to the left from $(i+1 \rightarrow i)$ under a negative effective stress, while negative dislocatoms show the opposite behavior. After a dislocatom has moved across a boundary, the dislocatom numbers on both sites are adjusted accordingly.

- Motion of a dislocatom across a boundary changes the strain associated with this boundary. If a dislocatom moves from a site under a positive effective stress, then the strain γ_{ij} on the crossed boundary is increased by $\rho_d b d$. If the dislocatom moves under a negative effective stress, the strain is decreased by the same amount.
- After a dislocatom has moved we re-calculate all stresses (for details see below) and determine the next critical boundary.

These rules implement a CA with extremal dynamics, corresponding to a physical situation where the velocity of dislocations increases with effective stress in a very abrupt manner (e.g. an exponential law with a large exponent or a very high power law), such that the dislocation with the highest stress moves much faster than all others. In this sense the CA dynamics provides an extreme contrast with the linear velocity law assumed in the continuum model.

B. Calculation of stresses

The effective driving stresses \mathcal{T}_{ij}^\pm are calculated from the same equations as for the transport model, with some adjustments for the discrete nature of the model and for the inclusion of stochastic terms. The total and excess dislocation densities are evaluated as $\rho_{ij} = \rho_d(n_{ij}^+ + n_{ij}^-)$ and $\kappa_{ij} = \rho_d(n_{ij}^+ - n_{ij}^-)$. The external stress is constant

throughout the system. Internal stresses are evaluated according to Eq. (6) with the convolution replaced by the discrete lattice sum. Back stresses and diffusion stresses are evaluated from Eqs. (8) and (9) with the spatial derivatives replaced by the respective directional difference quotients. The friction stress associated with the boundary (i, j) is evaluated as

$$\tau_{f,ij}^{\pm} = \alpha\mu b\sqrt{\rho_{ij} + \rho_{i+1,j}} \left(1 \mp \frac{\kappa_{ij} + \kappa_{i+1,j}}{\rho_{ij} + \rho_{i+1,j}} \right) * \xi_{ij}. \quad (13)$$

where ξ_{ij} is a Gaussian distributed random variable of average 1 and standard deviation σ_{τ} . After a dislocation move across some boundary, a new value of this variable is assigned to the boundary from the same distribution. This feature allows the model to account for stress fluctuations arising from the changes in local configurations of the discrete dislocations. Setting $\sigma_{\tau} = 0$ makes Eq. (13) the direct discrete counterpart of (11).

C. Initial conditions, boundary conditions, loading protocol

We impose periodic boundary conditions as in the continuum model. Initial conditions are constructed by placing $N \times N \times M/2$ positive and an equal number of negative dislocations randomly on the simulation lattice sites. We use two different types of loading protocol: (i) we impose a constant stress as in the continuum model. (ii) Alternatively, we increase, after an initial relaxation step, the stress precisely to the value needed to create one critical boundary. We trace the subsequent relaxation until no critical boundaries are left, and repeat. This algorithm corresponds to a quasi-static (infinitely slow) increase of the external stress and produces a stress-strain curve which approaches a horizontal asymptote corresponding to the macroscopic flow stress.

IV. RESULTS

A. Linear Stability Analysis of Transport Equations

A linear stability analysis (LSA) of the dislocation transport equations in Section 2 has been performed by Groma *et al.* [12]. Here we briefly summarize the results as a reference for comparison with the numerical investigation of the fully nonlinear equation and with the results obtained from the discrete stochastic model. One considers a spatially homogeneous reference state $\rho^+ = \rho^- = \rho_0/2$ under external stress τ_{ext} and investigates the time evolution of infinitesimal perturbations around this state in linear approximation. Because of the general scaling invariance properties of dislocation systems, results can be expressed in a generic form where all

dislocation densities are measured in units of $C_{\rho} = \rho_0$, all lengths in units of $C_l = \rho_0^{1/2}$, all times in units of $C_t = (M_0\mu b^2\rho_0)^{-1}$, all stresses in units of $C_{\tau} = \mu b\sqrt{\rho}$, and all strains in units of $C_{\gamma} = b\sqrt{\rho}$. In the following we use these units throughout.

Linear stability analysis leads to the following results:

- No plastic flow occurs and the dislocation microstructure is static for $\tau_{\text{ext}} \leq \alpha$.
- In the flowing phase ($\tau_{\text{ext}} > \alpha$), the growth rates of fluctuations follow from the equation

$$\Lambda^{\pm}(\mathbf{k}) = -\frac{(A+D)k_x^2 + T(\mathbf{k})}{2} \pm \frac{\sqrt{[(D+A)k_x^2 + T(\mathbf{k})]^2 - 4k_x^2[A(Dk_x^2 + T(\mathbf{k})) - B]}}{2} \quad (14)$$

where

$$B = \tau_{\text{ext}}[(3/2)\alpha - \tau_{\text{ext}}]. \quad (15)$$

- Within the unstable stress regime, there exists a band of unstable wave-vectors \mathbf{k} fulfilling the equation

$$ADk_x^2 + AT(\mathbf{k}) - B < 0. \quad (16)$$

Perturbations of maximum amplification have the wave-vector \mathbf{k}^{max} with $k_y^{\text{max}} = 0$ and

$$k_x^{\text{max}} = \rho_0^{1/2} \left[2B \frac{-1 + \sqrt{1 + \frac{(A-D)^2}{4AD}}}{(A-D)^2} \right]^{1/2}. \quad (17)$$

Hence, we expect the emerging patterns to be dominated by heterogeneities in x rather than y direction.

We now compare these predictions with solutions of the nonlinear transport equations, both for continuous transport and for discrete stochastic 'dislocation' dynamics.

B. Simulations of the continuum transport equations

Given that LSA predicts the dominant unstable mode to be associated with heterogeneities along the x but not the y direction, we first investigate a one-dimensional scenario where we impose homogeneity in y direction, hence $k_y = 0$ by construction. In x direction we use periodic boundary conditions with period $L = 500$. We consider two types of initial conditions, namely (i) a Gaussian white noise and (ii) a small, localized dislocation density 'blob' on top of the homogeneous background (Fig. 1). The amplitudes of the Fourier components of the perturbation are identical in both cases, however, in case of the

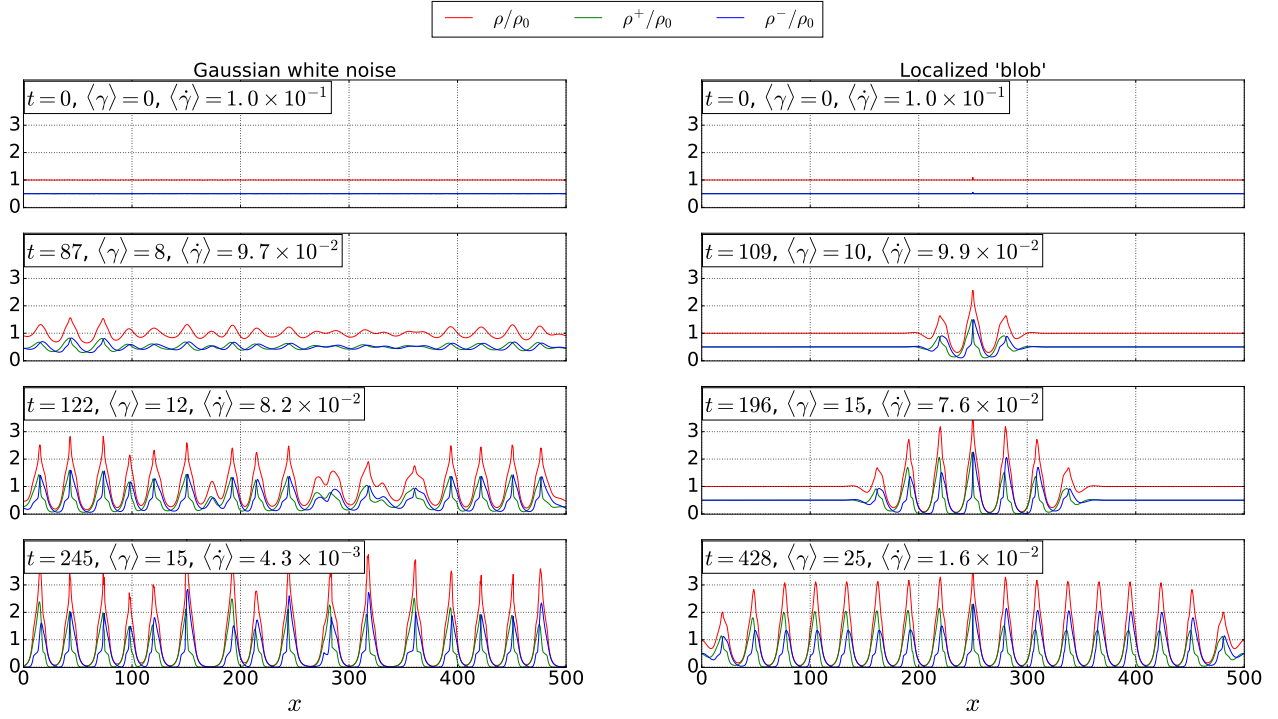


Figure 1. Spatio-temporal evolution of dislocation density patterns for two different initial conditions; left: small Gaussian white noise superimposed on a homogeneous density distribution, right: localized density fluctuation superimposed on a homogeneous distribution; parameters $A = 0.5$, $D = 0.4$, $\alpha = 0.3$, $\tau_{\text{ext}} = 1.1\alpha$.

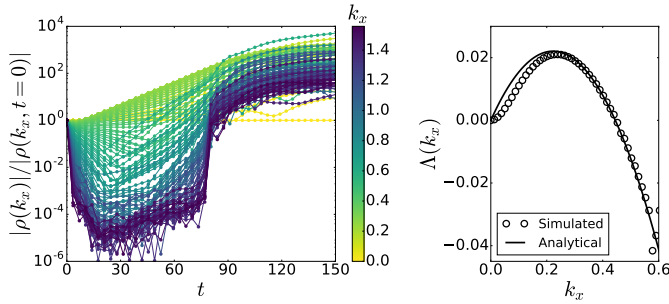


Figure 2. Left: Evolution of the Fourier modes $\rho(k_x)$ of the total dislocation density $\rho(x)$; right: growth rates as deduced from the initial slope of the $\ln |\rho(k_x)|$ vs t curves and analytical prediction according to Eq. (14); parameters as in Figure 1.

localized 'blob' the phases are identical whereas for the white noise they are random. Assuming a white noise perturbation leads to spatially distributed growth of the patterns, whereas a localized blob as initial condition leads to a correlated growth scenario where a fully developed pattern emerges locally and then spreads through propagation of an enveloping wave. Despite the different growth dynamics, the fully developed patterns resulting from initial conditions (i) and (ii) are very similar in terms of morphology and wavelength. The patterns consist of periodic walls of high dislocation density separated by dislocation depleted channels. The increased disloca-

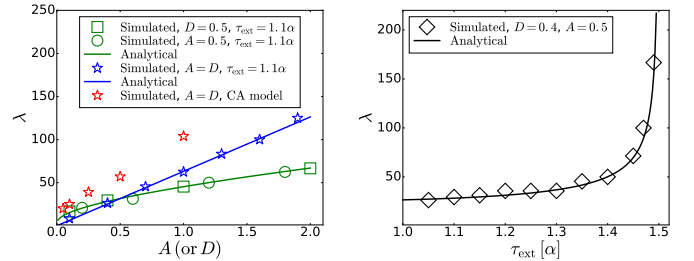


Figure 3. Pattern wavelength λ as a function of the model parameters, left: $\lambda(A, D)$ values for $D = 0.5$ (squares), $A = 0.5$ (circles) and $A = D$ (stars), solid line: theoretical curve according to Eq. (17) (note that this expression is symmetrical with respect to an exchange of A and D), $\tau_{\text{ext}} = 1.1\alpha$; right: $\lambda(\tau_{\text{ext}})$ for $A = 0.5$ and $D = 0.4$, solid line: theoretical curve according to Eq. (17).

tion density in the walls implies a high flow stress leading to piling up of positive dislocations on the left and of negative dislocations on the right side of the walls. The ensuing back stresses, in turn, reduce dislocation flow in the intermediate channels: Dislocation patterning is associated with a reduction in the overall strain rate.

Initially all Fourier modes of the perturbation have equal amplitude in both cases. The time evolution of the Fourier coefficients of the emergent patterns is shown in Fig. 2 (left) for case (i); case (ii) shows a practically

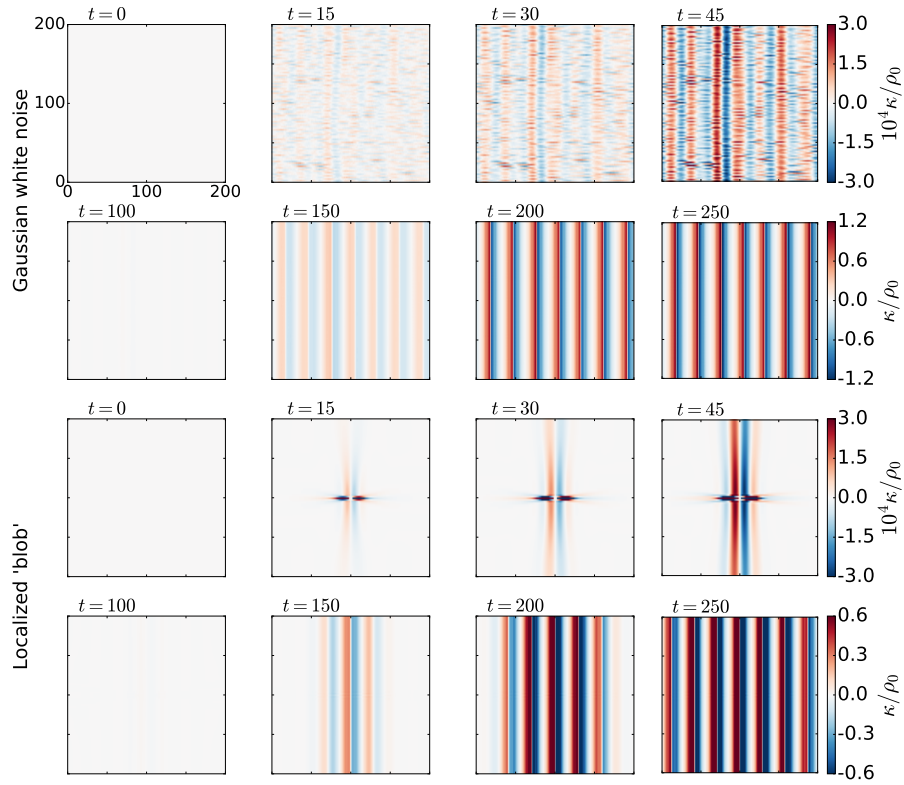


Figure 4. Spatio-temporal evolution of dislocation density patterns (excess density $\kappa(\mathbf{r})$) in two dimensions for two different initial conditions; upper two rows: small Gaussian white noise superimposed on a homogeneous density distribution; lower two rows: localized density fluctuation superimposed on a homogeneous distribution; parameters as in Figure 1.

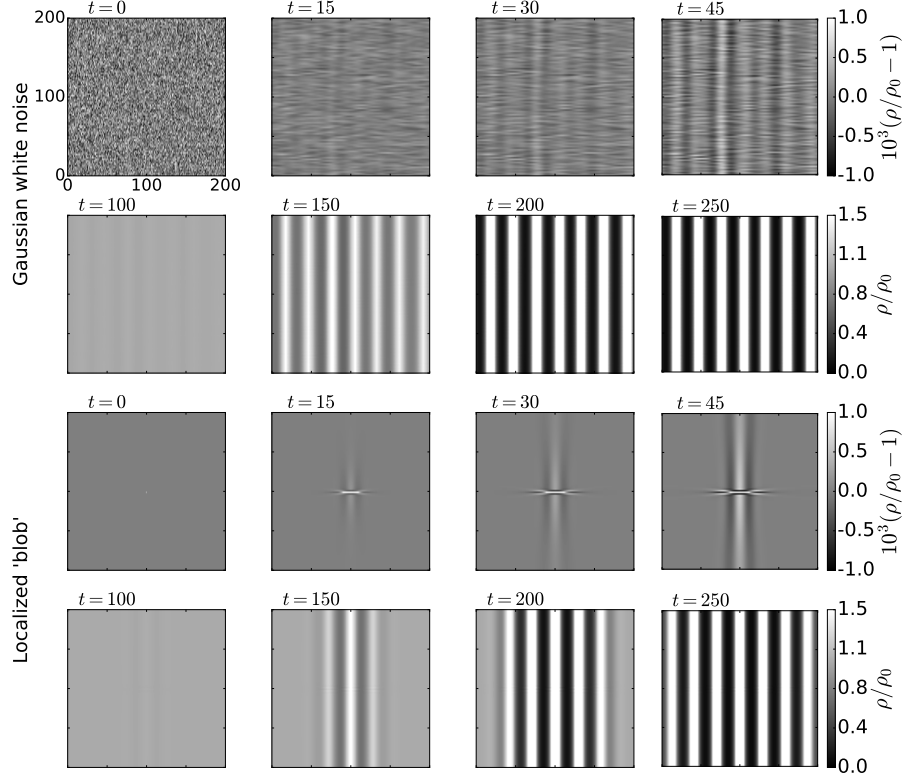


Figure 5. Spatio-temporal evolution of dislocation density patterns (total density $\rho(\mathbf{r})$) in two dimensions for two different initial conditions; upper two rows: small Gaussian white noise superimposed on a homogeneous density distribution; lower two rows: localized density fluctuation superimposed on a homogeneous distribution; parameters as in Figure 1.

identical behavior. From the initial growth rates of the discrete Fourier modes $\rho(k_x)$ we deduce growth factors defined as $\Lambda(k_x) = \Delta \ln \rho(k_x) / \Delta t$. Comparison with the analytical prediction of Eq. 14 shows excellent agreement as illustrated in Fig. 2 (right). The wavelengths of the fully developed patterns match very closely (within 5%) the predictions of linear stability analysis for the wavelength of the mode with maximum amplification. This observation, which holds throughout the parameter regime (Fig. 3), is remarkable since the nonlinearities have clearly a strong influence on the density distribution which is very different from a sinusoidal wave.

We then study the same patterning scenarios in two dimensions. In this case the emergent patterns have a stripe-like character where the system is near-homogeneous in y direction whereas the x dependency of the dislocation densities is almost identical to the one-dimensional case. If we use a Gaussian white noise as initial perturbation, embryonic patterns start growing locally and then, in a first 'synchronization' stage organize in y direction to form parallel walls. In a second 'growth' stage the amplitude of these wall like dislocation density modulations increases while the once-established pattern remains in place (Fig. 4 and Fig. 5, top). If, on the other hand, we start from a localized dislocation density 'blob' then an interesting scenario occurs (Fig. 4 and Fig. 5, bottom): The blob causes positive and negative dislocations to pile up from both sides. The long range stresses of the double pile up then lead to growth of a double wall similar to a kink band in y direction. Finally, the double wall serves as nucleus for a nonlinear wave which spreads the pattern in y direction as in the one dimensional case. Irrespective of the growth mode, the wavelength and morphology of the patterns are almost identical to the one dimensional case.

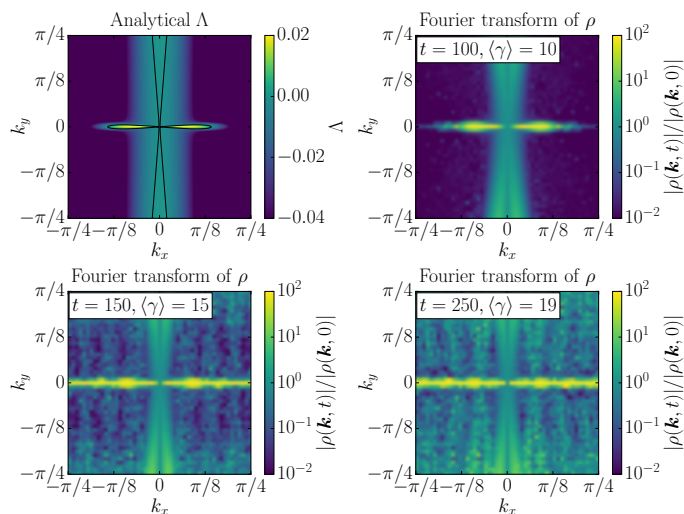


Figure 6. Top left: Analytical growth factor Λ as in Figure 2; top right: Normalized Fourier pattern $\rho(\mathbf{k}, t)$ for $t = 100C_t$, strain $\langle \gamma \rangle = 10$; bottom: Fourier patterns $\rho(\mathbf{k}, t)$ for $t = 150C_t$, strain $\langle \gamma \rangle = 15$ and $t = 250C_t$, $\langle \gamma \rangle = 19$; parameters as in Figure 1.

Finally, Fig. 6 shows the Fourier spectrum of the emerging dislocation density distribution. We use a logarithmic scale, hence the color level can also be envisaged as an exponential growth factor, enabling direct comparison with Fig. 6, top left. It can be seen that the Fourier pattern of the developing pattern closely matches the growth predictions of linear stability analysis also in 2D (Fig. 6, top right). At later stages, nonlinear effects lead to growth also of initially damped short-wavelength modes (Fig. 6, bottom). This is in close analogy with the 1D observations shown in Fig. 2, left. Note that the growth of damped modes concerns mainly harmonics in x of the initial unstable mode, as evidenced by the periodic striations of the Fourier patterns in Fig. 6, bottom.

C. Simulations of the stochastic cellular automaton model

Simulations of the stochastic cellular automaton model were conducted using a quasi-static stress increase protocol as described in Section III C with the dislocation size corresponding to $M = 16$. This leads to ascending stress strain curves reaching a horizontal asymptote (Fig. 7). Pattern formation is illustrated in Fig. 8. We can see

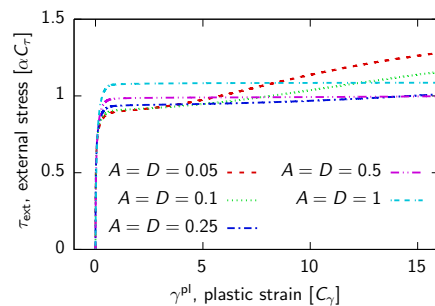


Figure 7. Stress-strain curves as obtained from the stochastic CA model under quasistatic loading conditions.

the emergence of alternating walls of positive and negative dislocations which become more pronounced with increasing strain.

The Fourier transform of the emergent patterns, taken at different strains, points to a growth scenario that differs substantially from that in the deterministic transport model. While the overall symmetry of the Fourier pattern matches the observations from the deterministic transport model and the corresponding linear stability analysis results, Fig. 9 demonstrates that the dominant wavelength of the patterns obtained from the CA shifts in the course of patterning from shorter to larger wavelengths (smaller k_x). This may be a feature of the short-wavelength noise that is inherent in the CA dynamics: The deterministic transport dynamics leads to a growth of the initially present spatial fluctuations that initially follows the LSA predictions. The CA dynamics, by contrast, continually adds spatio-temporal noise

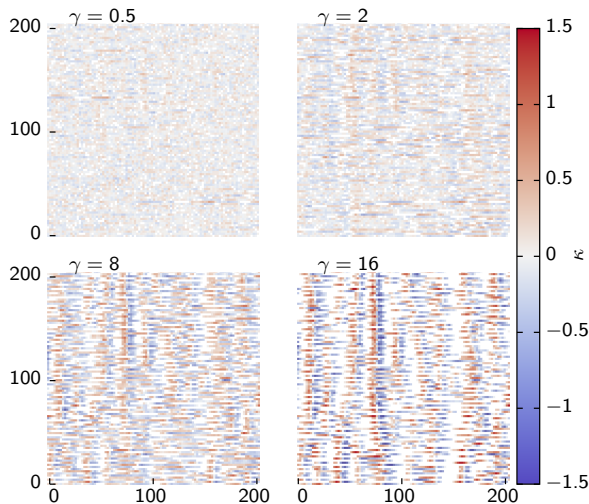


Figure 8. Spatio-temporal evolution of dislocation density patterns (excess density $\kappa(\mathbf{r})$) as obtained from the stochastic CA model using a quasi-static loading protocol; parameters $A = D = 0.1$, $\alpha = 0.3$.

at the shortest possible scale wavelength, namely on the scale of a single simulation cell.

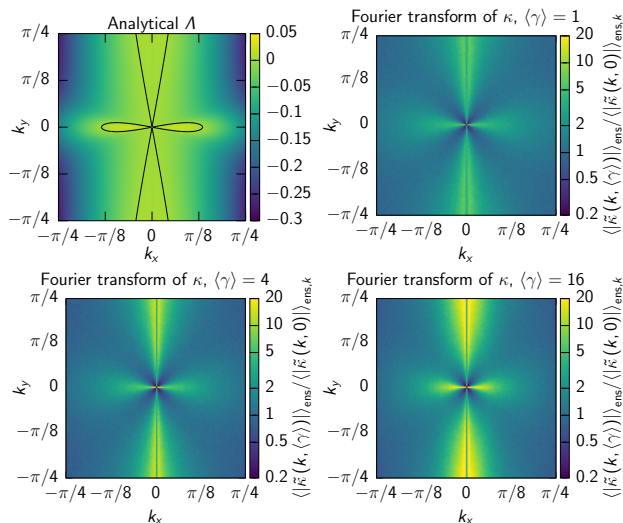


Figure 9. Top left: Analytical growth factor Λ according to Eq.(14) at $A=D=0.5$; top right: Normalized Fourier patterns $\kappa(\mathbf{k}, \gamma)$ for mean strain $\langle \gamma \rangle = 1$; bottom: Fourier patterns $\kappa(\mathbf{k}, \gamma)$ for mean strains $\langle \gamma \rangle = 4$ and $\langle \gamma \rangle = 16$, the Fourier patterns have been averaged over 100 realizations of the CA dynamics; cell size $d = 2$.

In agreement with the LSA the wavelength of the fully developed patterns increases with increasing A or D as illustrated by the stars in Fig. 3. However, at larger A or D values the characteristic wavelengths obtained are larger than it is predicted by the LDA. This can be attributed to the extremal dynamics used in the CA model. Moreover, the patterns obtained from the CA model are much

more 'noisy' than their deterministic counterparts. This is evident, for instance, from the absence of the higher order 'satellites' in the Fourier patterns of Fig. 9.

Repeating the simulations at constant external stress leads to results that are virtually identical with those derived from the quasi-static loading protocol. This is to be expected, since it is in the nature of the extremal dynamics that the addition of a constant stress, whatever its magnitude, does not change the sequence of events dictated by the extremal rule. As a consequence, the pattern wavelengths are stress independent: Whatever the stress level, the fully developed patterns match those obtained from the transport model in the limit $\tau_{\text{ext}} \rightarrow 1$ which represents the case of deformation at vanishing rate. This limit actually represents the physically relevant case since, in real patterning scenarios, the rate dependent contribution to the flow stress is exceedingly small. For illustration, we take typical parameters of Cu where $M_0 \approx 2 \times 10^4 \text{ Pa}^{-1} \text{ s}^{-1}$ (see Kubin and Canova [22]) and $b = 2.54 \times 10^{-10} \text{ m}$ and assume a dislocation density $\rho_0 = 10^{12} \text{ m}^{-2}$. A typical strain rate of 10^{-3} s^{-1} then requires a stress of the order of 1 Pa which is about 7 orders of magnitude below the typical level of the dislocation interaction stresses, hence, the characteristic deviation of the applied stress from the value $\tau_{\text{ext}} = 1$ is expected to be negligible.

V. CONCLUSIONS

Nonlinear simulations of a simple model of dislocation density patterning show that the fully developed patterns closely match the predictions derived from a simple linear stability analysis. The patterns depend little on the dynamical rules governing dislocation motion: Two different dynamic models, one assuming linearly stress dependent viscous dislocation motion and the other an extremely jerky cellular automaton evolution with extremal dynamics, produce qualitatively similar results. Also, simulations of the viscous model for different initial conditions show that the initial conditions, while having appreciable influence on the transient behavior, are practically immaterial to the fully developed pattern. In both viscous and CA models, patterning goes along with hardening as evidenced by a reduction in strain rate in the constant-stress viscous simulations or by an increase in stress in the CA simulations which use a quasi-static loading protocol. The final patterns are essentially governed by a quasi-static balance of the different stress contributions entering the model - they depend on a stress balance which makes dislocations rest in meta-stable configurations, but NOT on the way the dislocations move between such configurations. This provides some hints why dislocation patterns are similar in pure and solute hardened fcc metals, or in fcc metals and ionic crystals with KCl structure, where the dislocation velocity laws are surely very different.

Looking at the balance of stresses involved we see three

different kinds of stresses, which only in their mutual interplay can produce the observed patterning: First, we have an external stress driving the dislocation system. This is essential: no patterning can take place in the absence of plastic flow. Second, we have the stress contributions τ_{int} , τ_{back} and τ_{diff} which derive from an energy functional comprising elastic and defect energy contributions. These stresses are essential for understanding the pattern morphology and wavelength - in particular, the wall-like morphology of the patterns stems from the structure of the elastic energy functional and the corresponding stress kernel governing τ_{int} , whereas the pattern wavelength depends on the parameters A and D which control the defect energy contribution to the energy functional. It is, however, important to note that the internal energy related stress contributions alone can *not* explain pattern formation: In fact, the patterning process depends crucially on a fourth stress contribution which is dissipative in nature, namely the friction stress τ_f hence, the present patterning scenario cannot be envisaged as 'energetically driven'. In fact the basic mechanism leading to instability is simply the fact that, in a location of enhanced dislocation density, the friction stress is increased and hence more dislocations pile up in the same place. This is precisely the 'dynamic' patterning scenario of Nabarro [6], however, with the twist that without accounting for the 'energetic' stress contributions it is impossible to understand the pattern wavelength and pattern morphology!

We come thus to the conclusion that much of the past discussion about dislocation patterning may have been based upon false dichotomies and misleading analogies. Dislocation patterns are neither dynamic dissipative structures nor is their formation driven by energy minimization. Rather, the patterns emerge from the attempt

of the dislocation system to minimize a coarse grained energy functional while driven by an external stress and constantly encumbered by trapping into local, 'microscopic' energy minima which on the coarse grained scale appear as friction. Past analogies, be it with spinodal decomposition or dynamic chemical waves, have in our opinion not been very helpful to understanding this interplay. Nevertheless the use of metaphors for conceptualizing dislocation patterns has a long (if somewhat murky) tradition and we cannot help coming up with a metaphor of our own: We think that the emergence of metastable patterns from an interplay of driving, energy minimization and frictional 'shielding' resembles the processes governing the emergence of ripples on sand dunes: There, airflow over a sand surface and ensuing saltation provide the external driving force, gravity the potential energy that the system tries to minimize, and the screening of fluxes by already deposited grains the key mechanism that may lead to instability of a smooth sand surface with respect to ripple formation [23].

ACKNOWLEDGMENTS

M.Z and R.W acknowledge financial support by DFG within the framework of the research unit FOR1650 "Dislocation based plasticity" under grant No Za171/7-1. M.Z. also acknowledges support by the Chinese State Administration of Foreign Expert Affairs under Grant No MS2016XNJT044. IG and PDI have been supported by the National Research, Development and Innovation Fund of Hungary (project no. NKFIH-K-119561) and the Czech Science Foundation (PDI, project No. 15-10821S). PDI is also supported by the János Bolyai Scholarship of the Hungarian Academy of Sciences. Finally, we thank EC FP7 post-grant Open Access Pilot for financial support on article-processing charges.

-
- [1] N Hansen and D Kuhlmann-Wilsdorf, "Low-energy dislocation-structures due to unidirectional deformation at low-temperatures," *Mater. Sci. Eng.* **81**, 141–161 (1986).
 - [2] D. L. Holt, "Dislocation cell formation in metals," *J. Appl. Phys.* **41**, 3197–3201 (1970).
 - [3] D Walgraef and EC Aifantis, "Dislocation patterning in fatigued metals as a result of dynamical instabilities," *J. Appl. Phys.* **58**, 688–691 (1985).
 - [4] J. Pontes, D. Walgraef, and E. C. Aifantis, "On dislocation patterning: Multiple slip effects in the rate equation approach," *Int. J. Plasticity* **22**, 1486–1505 (2006).
 - [5] J. M. Salazar, R. Fournet, and N Banal, "Dislocation patterns from reaction-diffusion models," *Acta Metall. Mater.* **43**, 1127–1134 (1995).
 - [6] F.R.N. Nabarro, "Complementary models of dislocation patterning," *Philos. Mag. A* **80**, 759–764 (2000).
 - [7] T. Hochrainer, M. Zaiser, and P. Gumbsch, "A three-dimensional continuum theory of dislocation systems: kinematics and mean-field formulation," *Philos. Mag.* **87**, 1261–1282 (2007).
 - [8] Thomas Hochrainer, Stefan Sandfeld, Michael Zaiser, and Peter Gumbsch, "Continuum dislocation dynamics: Towards a physical theory of crystal plasticity," *J. Mech. Phys. Solids* **63**, 167–178 (2014).
 - [9] T. Hochrainer, "Multipole expansion of continuum dislocations dynamics in terms of alignment tensors," *Philos. Mag.* **95**, 1321–1367 (2015).
 - [10] I Groma, FF Csikor, and M Zaiser, "Spatial correlations and higher-order gradient terms in a continuum description of dislocation dynamics," *Acta Mater.* **51**, 1271–1281 (2003).
 - [11] P.L. Valdenaire, Y. Le Bouar, B. Appolaire, and A. Finel, "Density-based crystal plasticity: From the discrete to the continuum," *Phys. Rev. B* **93** (2016).
 - [12] Istvan Groma, Micihael Zaiser, and Peter Dusan Ispanovity, "Dislocation patterning in a two-dimensional continuum theory of dislocations," *Phys. Rev. B* **93** (2016).
 - [13] I. Groma, G. Gyorgyi, and B. Kocsis, "Dynamics of coarse grained dislocation densities from an effective free energy," *Philos. Mag.* **87**, 1185–1199 (2007).

- [14] Istvan Groma, Zoltan Vandruss, and Peter Dusan Ispanovity, “Scale-Free Phase Field Theory of Dislocations,” *Phys. Rev. Lett.* **114** (2015), 10.1103/PhysRevLett.114.015503.
- [15] M. Zaiser, “Local density approximation for the energy functional of three-dimensional dislocation systems,” *Phys. Rev. B* **92**, 174120 (2015).
- [16] T. Hochrainer, “Thermodynamically consistent continuum dislocation dynamics,” *J. Mech. Phys. Solids* **8**, 12–22 (2016).
- [17] Stefan Sandfeld and Michael Zaiser, “Pattern formation in a minimal model of continuum dislocation plasticity,” *Model Simul. Mater. Sc.* **23** (2015), 10.1088/0965-0393/23/6/065005.
- [18] Shengxu Xia and Anter El-Azab, “Computational modelling of mesoscale dislocation patterning and plastic deformation of single crystals,” *Model Simul. Mater. Sc.* **23** (2015), 10.1088/0965-0393/23/5/055009.
- [19] M. Sauzay and L. P. Kubin, “Scaling laws for dislocation microstructures in monotonic and cyclic deformation of fcc metals,” *Prog. Mater. Sci.* **56**, 725–784 (2011).
- [20] Michael Zaiser and Stefan Sandfeld, “Scaling properties of dislocation simulations in the similitude regime,” *Model Simul. Mater. Sc.* **22** (2014), 10.1088/0965-0393/22/6/065012.
- [21] M. Zaiser and P. Moretti, “Fluctuation phenomena in crystal plasticity—a continuum model,” *J. Stat. Mech-Theory E.* (2005), 10.1088/1742-5468/2005/08/P08004.
- [22] LP Kubin and G Canova, “The modeling of dislocation patterns,” *Scripta Metall.* **27**, 957–962 (1992).
- [23] J.F. Kok, E.J.R. Parteli, T.I. Michaels, and D. Bou Karam, “The physics of wind-blown sand and dust,” *Rep. Prog. Phys.* **75** (2012).